

Radio-frequency capacitive gate-based sensing

Imtiaz Ahmed,^{1,*} James A. Haigh,² Simon Schaal,³ Sylvain Barraud,⁴ Yi Zhu,⁵ Chang-min Lee,⁵ Mario Amado,⁵ Jason W. A. Robinson,⁵ Alessandro Rossi,¹ John J. L. Morton,^{3,6} and M. Fernando Gonzalez-Zalba^{2,†}

¹*Cavendish Laboratory, University of Cambridge,*

J. J. Thomson Ave., Cambridge, CB3 0HE, United Kingdom

²*Hitachi Cambridge Laboratory, J. J. Thomson Ave., Cambridge, CB3 0HE, United Kingdom*

³*London Centre for Nanotechnology, University College London, London, WC1H 0AH, United Kingdom*

⁴*CEA/LETI-MINATEC, CEA-Grenoble, 38000 Grenoble, France*

⁵*Department of Materials Science and Metallurgy, University of Cambridge,
27 Charles Babbage Road, Cambridge CB3 0FS, United Kingdom*

⁶*Department of Electronic & Electrical Engineering,
University College London, London WC1E 7JE, United Kingdom*

Developing fast, accurate and scalable techniques for quantum state readout is an active area in semiconductor-based quantum computing. Here, we present results on dispersive sensing of silicon corner state quantum dots coupled to lumped-element electrical resonators via the gate. The gate capacitance of the quantum device is configured in parallel with a superconducting spiral inductor resulting in resonators with loaded Q-factors in the 400-800 range. For a resonator operating at 330 MHz, we achieve a charge sensitivity of $7.7 \mu e/\sqrt{\text{Hz}}$ and, when operating at 616 MHz, we get $1.3 \mu e/\sqrt{\text{Hz}}$. We perform a parametric study of the resonator to reveal its optimal operation points and perform a circuit analysis to determine the best resonator design. The results place gate-based sensing at par with the best reported radio-frequency single-electron transistor sensitivities while providing a fast and compact method for quantum state readout.

I. INTRODUCTION

The spins of isolated electrons in silicon are one of the most promising solid-state systems on which to implement quantum information processing. With the recent demonstrations of long coherence times [1, 2], high fidelity spin readout [3], and one- and two-qubit gates [4–8], the basic requirements to build a quantum computer have been fulfilled [9]. Now, scaling the technology to a number of qubits sufficiently large to perform computationally relevant calculations is one of the major objectives and several proposals for large scale integration have been put forward [10–12]. In this respect, developing quantum state readout techniques that are fast and accurate while also being compact has become an active area of research.

Conventionally, readout in semiconductor gate-defined qubits is achieved using sensitive external electrometers. The most prominent example is the single-electron transistor (SET). Its radio-frequency version, the rf-SET [13], sets the standard as the most sensitive electrometer with the best charge sensitivity reported to date ($0.9 \mu e/\sqrt{\text{Hz}}$ [14]). The enhanced performance is based on reflectometry techniques that use lumped-element LC circuits to match the high-resistance of the detector to the 50Ω of the line [15]. However, mesoscopic electrometers, such as the rf-SET, need to be placed in close proximity to the qubits adding complexity to the circuit architecture.

Circuit quantum electrodynamics (QED) offers an alternative method for state readout of a quantum system. In this case, the qubit is embedded in a high Q-factor on-chip microwave resonator. This can be to the point of strong coupling, where the qubit and microwave photon dynamics become hybridized. In the dispersive limit, when the resonator and the quantum system are detuned, the state of the qubit can then be directly inferred from the oscillatory state of the resonator. This has been used to read superconducting [16] and more recently, semiconductor qubits [17–19].

The same principle of dispersive readout has also been applied to rf-reflectometry matching circuits [20–24]. This compact readout technique, namely in-situ gate-based readout, uses existing gate electrodes coupled to off-chip lumped-element resonators for sensing [20, 21]. This method alleviates the burden of external electrometers and reduces the complexity of the qubit architecture. Typically, gate-based sensing has been performed using low Q-factor resonators inspired by the matching networks developed for rf-SETs [20–24] and have not been optimized for reactive changes in device characteristics, such as the quantum or tunnelling capacitance [25–28].

Here, we bridge the gap between circuit QED type measurements and lumped-element reflectometry techniques, by optimizing external matching circuits for capacitive changes. We show that significant improvements in sensitivity are possible by changing the circuit topology to enhance the Q-factor of the resonator. While in one sense this brings rf-reflectometry towards conventional circuit QED, the fact that we keep the microwave circuitry separate means that it can be fabricated separately from the nanodevice. This allows independent nanofabrication strategies for the resonator and

* ia307@cam.ac.uk

† mg507@cam.ac.uk

the qubit. In particular, devices can be optimized to have a large coupling to the quantum system which is an important ingredient for the sensitive dispersive readout. This is where complementary metal-oxide-semiconductor (CMOS) technology, that for decades has been optimizing the gate coupling to the channel, can give an advantage over other qubit platforms.

In this paper, we report on in-situ dispersive readout of silicon-based CMOS few-electron quantum dots (QDs) [29, 30] using lumped-element classical resonators with loaded quality factors, Q_L , in the 400-800 range. The enhancement in Q_L is achieved by configuring the device gate capacitance in parallel with a superconducting spiral inductor and coupling via a coupling capacitor to a PCB coplanar waveguide. We find charge sensitivities of $7.7 \mu e/\sqrt{\text{Hz}}$ and $1.3 \mu e/\sqrt{\text{Hz}}$ for resonators operating at 330 MHz and 616 MHz, respectively. The latter represents an improvement of a factor of 30 over previous gate-based sensors [21] and sets gate-based reflectometry at par with the best ever reported rf-SETs. Finally, following a circuit analysis, we summarize the key requirements for sensitive capacitive gate-based readout: large Q_L resonators, well matched to the line, with low parasitic capacitance and large gate coupling to the quantum system. Our results pave the way for time-resolved dispersive readout of electron spin dynamics.

II. DEVICE AND RESONATOR

The device investigated is a CMOS silicon nanowire field-effect transistors (NWFET) with channel length $l = 30$ nm, width $w = 60$ nm and height $h = 11$ nm similar to the one shown in Fig. 1(a). The top-gate (tg) wraps around three faces of the n-type channel between the highly-doped source (s) and drain (d). At low temperatures, when the NWFET is biased below threshold ($V_{\text{tg}} \approx 0.5\text{V}$), few-electron QDs form in the NW channel [29, 31]. The transistor's multigate geometry, combined with a small equivalent gate oxide thickness of 1.3 nm, results in QDs with large gate couplings $\alpha = C_{\text{tg}}/C_{\Sigma} = 0.85 - 0.89$ since the total capacitance C_{Σ} is mostly given by its capacitance to the gate electrode C_{tg} .

The device is embedded in an electrical resonator containing a polycrystalline NbN superconducting planar spiral which provides a low-loss and low self-capacitance inductor L [20, 32, 33]. The 80 nm NbN films were grown in unheated c-plane $430 \mu\text{m}$ thick sapphire substrates by DC magnetron sputtering. The deposition was done in an Ar/N₂ atmosphere with 28% N₂ at 1.5 Pa. The spiral was defined using optical lithography and etching, see Fig. 1(b). We wirebonded the inductor in parallel to the device gate capacitance to ground, C_d , and the circuit parasitic capacitance, C_p , and coupled to the Z_0 line via a coupling capacitor C_c as shown in Fig. 1(c). This differs from the series configuration explored in Refs. [20-24] and, as we shall see later, leads to enhanced sensitiv-

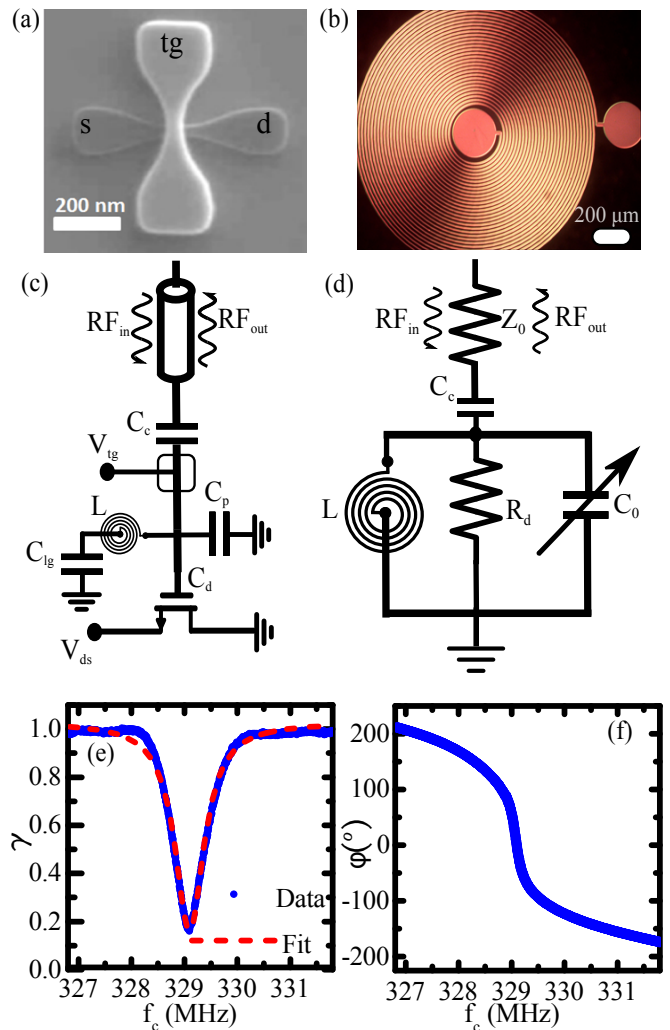


FIG. 1. Device and resonator. (a) A scanning-electron micrograph of a NWFET showing source (s), drain (d) and top-gate (tg) terminals. (b) Optical image of a superconducting NbN spiral inductor. The spiral track width and track spacing are both $8 \mu\text{m}$. (c) Circuit diagram for rf-reflectometry. The NbN inductor L is connected in parallel with the top-gate of the NWFET. The circuit has a parasitic capacitance of C_p to ground. V_{ds} and V_{tg} are the bias voltages. $C_{\text{lg}} = 100$ pF. (d) Model for the parallel resonator coupled to external line impedance $Z_0 = 50 \Omega$ through C_c . The resistor R_d represents the losses in the resonator. (e) Amplitude γ of the reflection coefficient Γ measured (blue) and fit (red). (f) Phase ϕ of the reflection coefficient Γ .

ity to capacitance changes. A simple equivalent model for the resonator, as in Fig. 1(d), consists of L , the circuit losses R_d and the variable capacitor $C_0 = C_p + C_d$ placed in parallel and coupled to the line by C_c . R_d represents dielectric losses in the device and the PCB, and can contain dissipative terms arising from Sisyphus processes [21, 26, 27, 34]. The parasitic capacitance, C_p , combines contributions from the device and the PCB.

In order to characterize the resonant frequency f_0 ,

bandwidth BW and Q_L , we measure the complex reflection coefficient $\Gamma = \gamma e^{i\phi}$ as a function of the carrier frequency f_c . In Fig. 1(e), we show the magnitude γ (in blue) and a fit (in red). From this we estimate $L = 405$ nH, $C_c = 90$ fF, $C_p = 480$ fF, $R_d = 800$ k Ω . This gives us $f_0 = 1/(2\pi\sqrt{L(C_c + C_0)}) = 329.33$ MHz, $Q_L \approx 400$ and BW = 0.82 MHz. The large depth of the resonance, $\gamma_{min} = 0.168$ indicates that the resonator is close to matching. The loaded Q contains contributions from the external Q-factor, $Q_e = (C_c + C_0)/2\pi f_0 Z_0 C_c^2 = 680$, and the unloaded Q-factor of the resonator, $Q_0 = 2\pi f_0 (C_c + C_0) R_d = 943$. In this particular design, external losses dominate Q_L but its value is increased by an order of magnitude when compared to series resonator gate-based approaches [20–24]. We operate in the over-coupled regime confirmed by the 180° phase shift, ϕ , as a function of carrier frequency in Fig. 1 (e).

III. DISPERSIVE REGIME

Gate-based sensing is a resonant technique that allows probing the complex admittance of a quantum device [20, 26, 35, 36]. Here, we couple a single QD in the NW channel to the resonator and probe its impedance using gate-based radio-frequency reflectometry at 40 mK [37, 38]. We use this to probe susceptibility changes when adiabatic single-electron tunneling occurs between the QD and the s/d reservoirs. At resonance, variations in ϕ capture changes in the device capacitance ΔC that can be attributed to tunneling or quantum capacitance [28]. Since the resonator is over-coupled, $\Delta\phi = -2Q_L\Delta C/(C_c + C_0)$.

In our system, the origin of ΔC can be explained by considering an uncoupled two level system (TLS) described by a QD with zero (E_0) or one excess electron (E_1). Particles are exchanged with the s/d reservoirs. If the TLS is driven by an external sinusoidal excitation at f_0 and the relaxation rate ν between levels is comparable, Sysiphus dissipation occurs [21, 27]. However, if $\nu \gg f_0$, electrons tunnel adiabatically and out of phase with the drive. This results in a purely dispersive signal manifesting as a tunneling capacitance contribution C_t [22]. In Fig. 2(a), we show schematically a TLS driven across a charge degeneracy point where E_0 and E_1 cross each other at a fixed top-gate voltage point V_{tg}^0 . In the regime $\nu \gg f_0$, the electron always stays in the ground state and the tunneling capacitance is given by

$$C_t = \frac{(\alpha e)^2}{\pi} \frac{h\nu}{(h\nu)^2 + (\alpha e \Delta V_{tg})^2}, \quad (1)$$

where h is the Planck's constant, e is the electron charge and $\Delta V_{tg} = V_{tg} - V_{tg}^0$ [22, 39]. This voltage-dependent C_t produces a phase shift in the resonator as can be seen in Fig. 2 (b) where $\Delta\phi$ is plotted as the V_{tg} is swept across the charge degeneracy point. We measure a maximum phase shift $\Delta\phi = 28^\circ$ at the degeneracy point. Using

Eq. (1), we fit $\Delta\phi$ (red curve) and extract $\nu = 26$ GHz ($\gg f_0$) from the full-width-half-maximum (FWHM). C_t loads the resonator pulling down its resonant frequency as shown in Fig. 2(c). Finally, in Fig. 2(d,e), we compare γ and ϕ on and off the degeneracy point. From these measurements we extract a dispersive shift $\Delta f = 88$ kHz, which corresponds to an effective change in capacitance given by $\Delta C = 2(C_c + C_0)\Delta f/f_0 = 0.3$ fF. This agrees well with the expected maximum tunneling capacitance 0.37 fF, calculated from Eq. (1).

IV. CHARGE SENSITIVITY

We use the conventional technique [13] to measure the charge sensitivity of the capacitive gate-based sensor: A small sinusoidal voltage is applied to the top-gate of the device with a root mean square charge equivalent amplitude Δq and frequency f_m . This produces an amplitude modulation of the carrier that results in sidebands appearing in the power spectrum of the reflected signal at $f_c \pm f_m$, as can be seen in Fig. 3(a) along with the rf carrier. The height of the sideband measured from the noise floor defines the power signal-to-noise ratio (SNR). The charge sensitivity is then calculated from the definition, $\delta q = \Delta q / (\sqrt{2\text{RBW}} \times 10^{\frac{\text{SNR}}{20}})$ where RBW is the resolution bandwidth of the spectrum analyzer [14]. A separate figure of merit is the modulation depth dBc, given by the sideband height relative to the carrier in dB. This figure indicates how much of the input signal is modulated by the device.

Fig. 3(a) shows the power spectrum at the optimal working point of the resonator (identified by measurements described below). The spectrum is obtained using a modulation signal with $f_m = 511$ Hz and $\Delta q = 6.98 \times 10^{-3}e$ and a RBW = 10 Hz. We measure a SNR=26.1 dB, resulting in $\delta q = 7.7 \mu e/\sqrt{\text{Hz}}$. This result represents a charge sensitivity improvement of a factor of ~ 5 with respect to previous reports [21] and demonstrates the advantage of adopting the circuit configuration of the capacitive gate sensor.

We now discuss the parametric study of the gate-based sensor's sensitivity in terms of V_{tg} , f_c and carrier power P_c to find the optimal working point. In Fig. 3(b), we show the lower sideband SNR as a function of V_{tg} and P_c . For a fixed P_c , the SNR shows two maxima whose separation in V_{tg} increases as P_c is increased. The position of the maxima corresponds to the V_{tg} points of maximum slope at either side of the charge transition in Fig. 2(b). The dependence of the separation with increasing P_c indicates that the transition is being broadened by the rf voltage V_c . Only at the lowest values of P_c , where the separation between peaks remains constant, is the transition lifetime limited.

To find the optimal carrier power for sensing, we extract the maximum SNR at each P_c (blue dots) as shown in Fig. 3(c). The SNR peaks at $P_c = -98$ dBm when the transition is still power broadened, as opposed to the

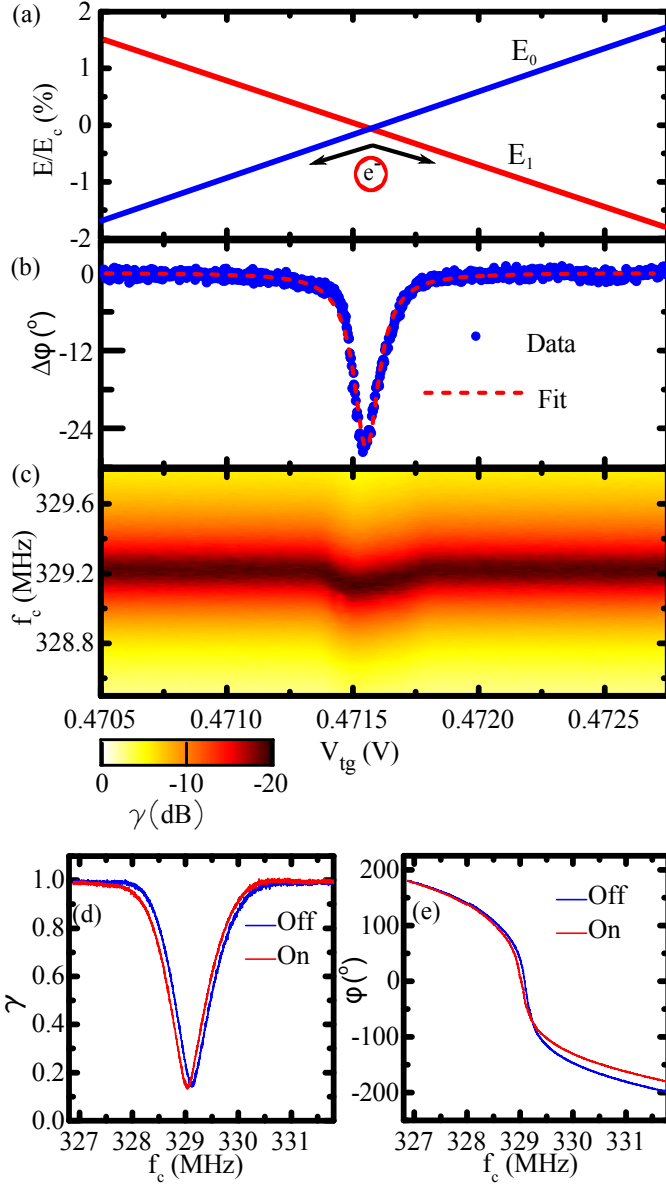


FIG. 2. Dispersive regime. (a) Energy diagram of a fast driven TLS, E_0 and E_1 , across a charge degeneracy point. The energy is normalized to charging energy E_c of the QD. (b) Data (blue dot) and Lorentz fit (red dashed line) for the phase change $\Delta\phi$ of the resonator as a function of V_{tg} . (c) γ as function of carrier frequency f_c and V_{tg} . Experimental data for γ (d) and ϕ (e) at two different V_{tg} voltages - away from and at the charge degeneracy, blue and red traces respectively.

expectation that the maximum SNR would be achieved when the transition is lifetime broadened. To understand why, we define the modulation index $M = 10^{\frac{\text{dBc}}{20}}$ and note that the sideband SNR can be expressed as $\text{SNR} = M \times P_c$. M decreases as the rf carrier voltage V_c increases as seen in Fig. 3(d). This dependence can be modeled as a convolution of two competing processes: lifetime broadening and power broadening. The transi-

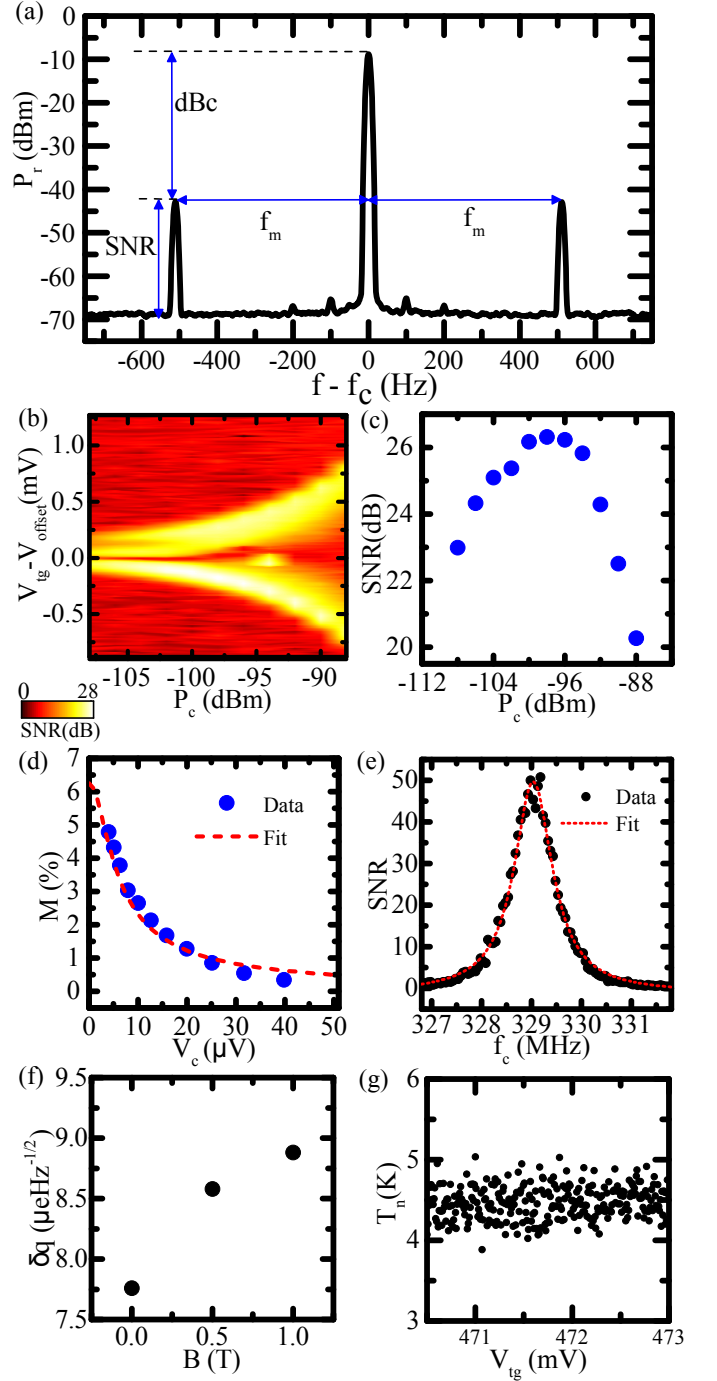


FIG. 3. Measuring and optimizing charge sensitivity. (a) Reflected power P_r spectrum showing the sidebands at $f_c \pm f_m$ due to gate-voltage modulation. (b) SNR in dB as a function of V_{tg} and P_c ($V_{\text{offset}} = 472.23$ mV). (c) Sideband SNR as function of P_c . (d) Modulation index M (blue dots) and fit (red dashed line) as a function of input rf carrier voltage V_c . (e) Sideband power SNR in linear scale vs. rf-carrier frequency f_c measured at $P_c = -115$ dBm. (f) Measured charge sensitivity as a function of the magnetic field B . (g) Noise temperature T_n as a function of V_{tg} measured at f_0 with RBW=300 kHz.

tion is lifetime broadened by ν to produce a linewidth V_ν ($h\nu = e\alpha V_\nu$) and power broadened by applied rf carrier power with a linewidth proportional to V_c . The dependence of M on V_c can be approximated by $1/\sqrt{V_\nu^2 + V_c^2}$ which decreases with increasing V_c as shown in Fig. 3(e) (red dashed curve). The maximum SNR occurs when the increase in input power is compensated by the decrease in M .

Next, we find the optimal carrier frequency. We plot the sideband power SNR (in linear scale) at $f_c - f_m$ as a function of rf carrier frequency f_c when swept across a frequency range containing f_0 (see Fig. 3(e)). The SNR shows a Lorentzian profile with center frequency f_0 , and BW and Q_L matching the values obtained from Fig. 1(e). To avoid power broadening, the input RF power was kept at -115 dBm during this measurement.

Additionally, we study the dependence of the sensor's charge sensitivity on in-plane magnetic field, given our use of a superconducting material (NbN) for the lumped element inductor, and the fact that for typical spin qubit systems, an external magnetic field is used to Zeeman-split the spin degenerate energy levels [3, 4, 40]. We measured SNR = 24.9 dB at 1 T which gives a charge sensitivity $\delta q = 8.8 \mu e/\sqrt{\text{Hz}}$ as shown in Fig. 3(f). This result demonstrates that our gate-sensor sensitivity only deteriorates by 15% at 1 T and hence is robust against moderate magnetic fields used to operate Si spin qubits.

Finally, in Fig. 3(g), we measure the noise temperature T_n of the system at the resonance frequency as a function of V_{tg} . As we sweep V_{tg} across the charge degeneracy point, T_n stays constant 4.5 ± 0.4 K which matches with the noise temperature of our cryogenic amplifier (Quinstar QCA-U350-30H). Hence we conclude that charge sensitivity is limited by the thermal noise of the cryo-amplifier and not by Sisyphus noise which can be orders of magnitude smaller [21]. In this study, we emphasize the importance of improving the resonator design to increase the signal of gate-based approaches. Improving the noise floor by using, for example, a Josephson Parameter Amplifier (JPA) will lead to additional enhancements on the experimental sensitivity of the capacitive gate-based sensor.

V. RESONATOR OPTIMIZATION

In this section, we explore the resonator design analytically to highlight ways to optimize the circuit and understand the ultimate performance of capacitive gate-based charge sensing. We consider the circuit in Fig. 1(d) and its reflection coefficient:

$$\Gamma = \frac{Z - Z_0}{Z + Z_0}, \quad (2)$$

where Z is the complex impedance of the coupling capacitor C_c in series with the parallel combination of the inductor L , the circuit resistance R_d and circuit variable

capacitance C_0 . Gate-based reflectometry is sensitive to changes in the reflection coefficient. In this work, we are concerned with capacitance changes in the circuit due to single-electron tunneling that can manifest in the form of quantum or tunneling capacitance [28]. Therefore, we calculate the absolute value of the differential change in reflection coefficient with C_0 ,

$$|\Delta\Gamma| = \left| \frac{\partial\Gamma}{\partial C_0} \Delta C \right| = \frac{2R_{\text{eq}}Z_0}{(R_{\text{eq}} + Z_0)^2} Q_0 \frac{\Delta C}{C_c + C_0} \quad (3)$$

Here, $R_{\text{eq}} = L(C_c + C_0)/R_d C_c^2$, is the equivalent resistance of the circuit at $f = f_0$, as depicted in Fig. 4(a). The charge sensitivity is inversely proportional to $|\Delta\Gamma|$ and hence a study of this magnitude yields an estimate of the relative sensitivity level [41, 42].

Eq. 3 provides the guidelines to optimize the sensitivity of gate-based sensing approaches. Firstly, exemplified in Fig. 4(b), where we plot both $|\Delta\Gamma|$ and Γ as a function of C_c , we observe that $|\Delta\Gamma|$ is maximum when the coupling capacitor is chosen to give perfect matching ($\Gamma = 0$) i.e. $R_{\text{eq}} = Z_0$. Secondly, increasing R_d , and in turn the unloaded Q-factor, leads to an increase in sensitivity. The effect on $|\Delta\Gamma|$ of increasing R_d can be seen in Fig. 4(c) where the maximum $|\Delta\Gamma|$ increases as R_d is increased from 200 k Ω (blue) to 2 M Ω (black). Note the change in optimal C_c as R_d is varied. $|\Delta\Gamma|_{\text{max}}$ increases linearly with R_d as can be seen in the inset. Thirdly, a reduction of the circuit capacitance, by reducing C_p , leads to an enhanced sensitivity. This can be observed in Fig. 4(c) where we plot $|\Delta\Gamma|$ as a function of C_c and fixed L and R_d for three different values of C_p , 0.2 pF (black), 0.48 pF (red) and 0.8 pF (blue). $|\Delta\Gamma|_{\text{max}}$ decreases as $C_p^{-1/2}$, as can be seen in the inset. Finally, the change in device capacitance, ΔC , needs to be maximized. This can be achieved by maximising the gate coupling factor α which has a quadratic effect on $|\Delta\Gamma|$ as can be seen in Eq. (1).

Ultimately, Eq. 3 can be expressed in much simpler terms when the resonator is matched to the line, $|\Delta\Gamma| = \pi R_d f_0 \Delta C$. In this case, we see that the optimal device should have as low dissipation as possible (large R_d). Moreover, gate-based sensing benefits from operating at high frequency as we demonstrate in the next Section.

VI. HIGHER FREQUENCY OPERATION

To assess the advantage of operating the capacitive gate-based sensor at higher frequencies, we perform a second set of experiments on a nominally identical device but narrower channel, $w = 30$ nm, and a resonator with resonant frequency $f_0 = 616.18$ MHz. We use a NbN inductor, $L = 134$ nH. In Fig. 5(a,b), we see the magnitude γ and phase ϕ of the reflection coefficient. The resonator has a $BW = 0.78$ MHz and hence a loaded Q-factor $Q_L = 790$, is close to matching $\gamma_{\text{min}} = 0.1$ and overcoupled $Q_e < Q_0$.

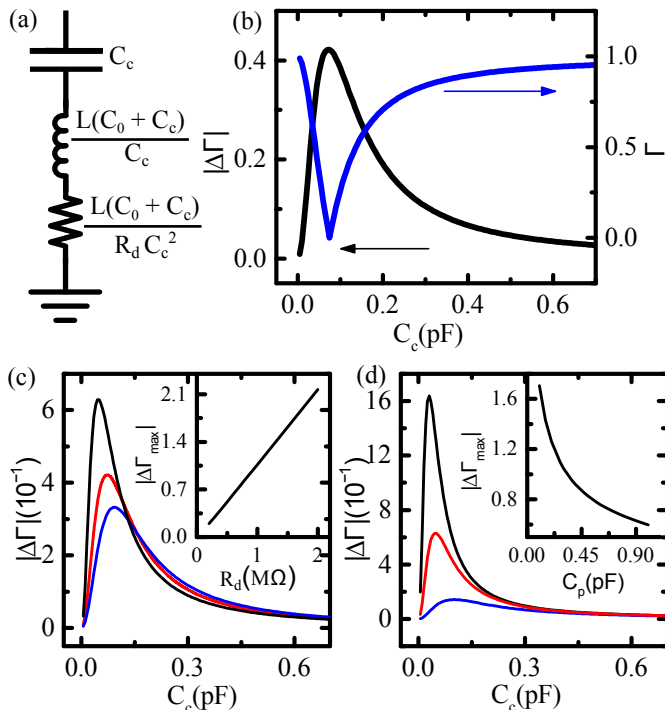


FIG. 4. Resonator optimization. (a) Equivalent circuit at resonance. (b) $|\Delta\Gamma|$ (black) and Γ (blue) as a function of C_c for the experimental values $R_d = 800$ k Ω , $C_p = 0.48$ pF and $L = 405$ nH, $Z_0 = 50$ Ω . We consider $\Delta C = 1$ fF. (c) Dependence on R_d . $|\Delta\Gamma|$ as a function of C_c for $R_d = 200$ k Ω (blue), 800 k Ω (red) and 2 M Ω (black). Inset: Maximum $|\Delta\Gamma|$ as a function of R_d . (d) (c) Dependence on C_p . $|\Delta\Gamma|$ as a function of C_c for $C_p = 0.8$ pF (blue), 0.48 pF (red) and 0.2 pF (black). Inset: Maximum $|\Delta\Gamma|$ as a function of C_p .

We characterize the gate-based sensor in terms of charge sensitivity following the procedure explained in Section IV and obtain an optimized charge sensitivity of $1.3 \mu e/\sqrt{\text{Hz}}$ at $P_c = -120$ dBm. For this measurement, we use $\Delta q = 1.48 \times 10^{-4} e$ and RBW = 20 Hz. The sensitivity improvement is ≈ 30 when compared to previous reports [21] and places the charge sensitivity of the capacitive gate-based sensors on a par with the best reported rf-SET sensitivities [14, 43].

We demonstrate the advantage of the improved sensitivity by acquiring a charge stability map of the device containing 512×256 data points in just 700 ms, see Fig. 5(c). Here, we use a double ramp scheme [44] where we ramp the drain voltage, V_{ds} at 4 kHz (sawtooth) while slowly ramp V_{tg} at 7 Hz (triangular). The frequency of the ramp is limited in this measurement by the low-pass filtering in our lines (cut-off frequency 5 kHz). The 2D map is composed of traces of the demodulated phase response. In Fig. 5(c), we see the characteristic signature of Coulomb Blockade measured dispersively with the gate-based sensor. The combination of the data quality and short acquisition time demonstrates the potential of this new gate-based sensor design for fast readout of semiconductor nanostructures. Given the integration time of

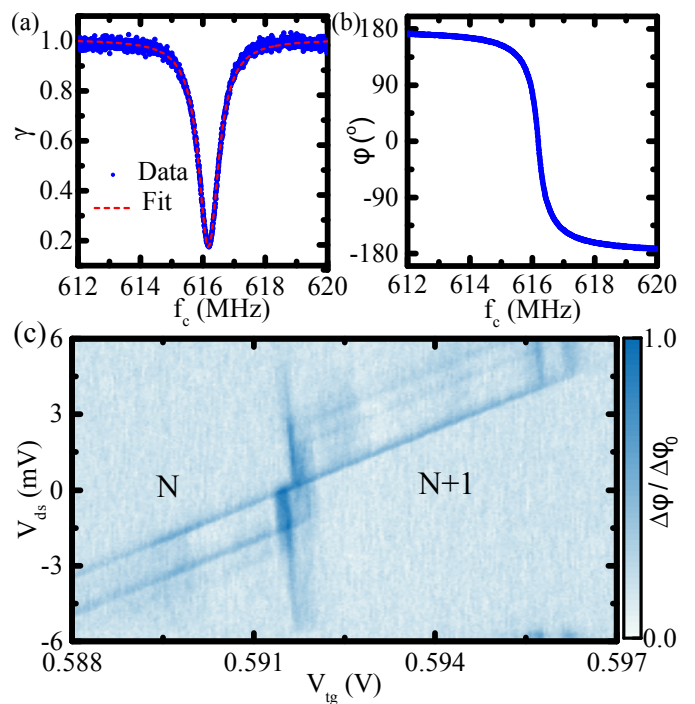


FIG. 5. High frequency resonator. Magnitude (a) and phase (b) of the reflection coefficient Γ as a function of frequency. (c) Fast data acquisition of a dot to reservoir transition. V_{ds} was ramped at 4 kHz while V_{tg} at 7 Hz. Each trace was averaged 5 times. The total measurement time is 700 ms.

$5 \mu\text{s}$ per point, capacitive gate-based sensing may enable performing single-shot readout of electron spin dynamics in silicon.

VII. CONCLUSION

We have demonstrated an optimized design for in-situ gate-based sensing for which the charge sensitivity is a factor of 28 better than the best reported gate-sensor [21] and it is comparable to the best sensitivities ever demonstrated for the RF-SET [14]. In the case of the RF-SET the experimental sensitivity is limited by shot-noise whereas in the case of our gate-sensor is limited by the noise of the cryogenic amplifier. Hence by using a quantum-limited amplifier, a gate-sensors with sub $\mu e/\sqrt{\text{Hz}}$ sensitivity will be possible, making the gate-sensor the most sensitive electrometer. The ultimate sensitivity of this dispersive sensor remains to be explored and a study should consider the effects of the Sisyphus noise [21] and the Johnson-Nyquist noise of the resonator which can be orders of magnitude lower than shot-noise at milliKelvin temperatures and radio-frequencies. Additionally, the charge sensitivity demonstrated combined with the bandwidth of the resonators results in a few microsecond detection with an rms charge noise ($\Delta Q = \delta q \times \sqrt{\text{BW}}$) well below $1 e$. Therefore, capacitive gate-based sensing could allow single-shot readout

of electron spins in silicon double QDs where the relaxation and coherence times are typically larger than a microsecond [1, 2]. In the future, devices with additional gates such as CMOS transistors in series [45] or split-gate CMOS transistors [46, 47] should provide access to experiments in which the resonator couples to an interdot charge transitions and Pauli spin blockade is used for electron spin readout.

VIII. ACKNOWLEDGMENTS

We thank Ferdinand Kuemmeth and Andrew J. Ferguson for useful comments. This research has received funding from the European Union's Horizon 2020 Re-

search and Innovation Programme under grant agreement No 688539 (<http://mos-quito.eu>) and No. 732894 (<http://hot-fetpro.eu>); as well as by the Engineering and Physical Sciences Research Council (EPSRC) through the Centre for Doctoral Training in Delivering Quantum Technologies (EP/L015242/1) and UNDEDD (EP/K025945/1), and the Winton Programme of the Physics of Sustainability. I.A. is supported by the Cambridge Trust and the Islamic Development Bank. A. R. acknowledges support from the European Union's Horizon 2020 research and innovation programme under the Marie Skłodowska-Curie grant agreement No 654712 (SINHOPSI). J.W.A.R. acknowledges funding from the Royal Society and M.A. the EPSRC through the Programme Grant EP/N017242/1 and EP/P026311/1.

-
- [1] M. Veldhorst, J. Hwang, C. Yang, L. A.W., B. de Ronde, J. P. Dehollain, J. Muhonen, F. Hudson, K. Itoh, A. Morello, and A. S. Dzurak, *Nature* **9**, 981 (2014).
- [2] E. Kawakami, P. Scarlino, D. Ward, F. Braakman, D. Savage, M. Lagally, M. Friesen, S. Coppersmith, M. Eriksson, and L. Vandersypen, *Nature nanotechnology* **9**, 666 (2014).
- [3] A. Morello, J. J. Pla, F. A. Zwanenburg, K. W. Chan, K. Y. Tan, H. Huebl, M. Mottonen, C. D. Nugroho, C. Yang, J. A. van Donkelaar, A. D. C. Alves, D. N. Jamieson, C. C. Escott, L. C. L. Hollenberg, R. G. Clark, and A. S. Dzurak, *Nature* **467**, 687 (2010).
- [4] M. Veldhorst, C. H. Yang, J. C. C. Hwang, W. Huang, J. P. Dehollain, J. T. Muhonen, S. Simmons, A. Laucht, F. E. Hudson, K. M. Itoh, A. Morello, and A. S. Dzurak, *Nature* **526**, 410 (2015).
- [5] E. Kawakami, T. Jullien, P. Scarlino, D. R. Ward, D. E. Savage, M. G. Lagally, V. V. Dobrovitski, M. Friesen, S. N. Coppersmith, M. A. Eriksson, and L. M. K. Vandersypen, *Proceedings of the National Academy of Sciences* **113**, 11738 (2016).
- [6] D. Zajac, A. Sigillito, M. Russ, F. Borjans, J. Taylor, G. Burkard, and J. Petta, *Science*, eaa05965 (2017).
- [7] J. Yoneda, K. Takeda, T. Otsuka, T. Nakajima, M. R. Delbecq, G. Allison, T. Honda, T. Kodera, S. Oda, Y. Hoshi, N. Usami, K. M. Itoh, and S. Tarucha, *Nature nanotechnology*, 1 (2017).
- [8] T. F. Watson, "A programmable two-qubit quantum processor in silicon," *ArXiv:1708.04214*.
- [9] D. P. DiVincenzo, *Fortschritte Der Physik-Progress of Physics*, **48**, 771 (2000).
- [10] L. M. K. Vandersypen, H. Bluhm, J. S. Clarke, A. S. Dzurak, R. Ishihara, A. Morello, D. J. Reilly, L. R. Schreiber, and M. Veldhorst, *npj Quantum Information* **3**, 34 (2017).
- [11] M. Veldhorst, H. G. J. Eenink, C. H. Yang, and A. S. Dzurak, *Nature Communications* **8**, 1766 (2017).
- [12] R. Li, "A crossbar network for silicon quantum dot qubits," *ArXiv:1711.03807*.
- [13] R. Schoelkopf, P. Wahlgren, A. Kozhevnikov, P. Delsing, and D. Prober, *Science* **280**, 1238 (1998).
- [14] H. Brenning, S. Kafanov, T. Duty, S. Kubatkin, and P. Delsing, *Journal of Applied Physics* **100**, 114321 (2006).
- [15] D. Reilly, C. Marcus, M. Hanson, and A. Gossard, *Applied Physics Letters* **91**, 162101 (2007).
- [16] A. Wallraff, D. I. Schuster, A. Blais, L. Frunzio, J. Huang, R. S. and Majer, S. Kumar, S. M. Girvin, and R. J. Schoelkopf, *Nature* **431**, 162 (2004).
- [17] K. D. Petersson, L. W. McFaul, M. D. Schroer, M. Jung, J. M. Taylor, A. A. Houck, and J. R. Petta, *Nature* **490**, 380 (2012).
- [18] A. Stockklauser, P. Scarlino, J. V. Koski, S. Gasparinetti, C. K. Andersen, C. Reichl, W. Wegscheider, T. Ihn, K. Ensslin, and A. Wallraff, *Phys. Rev. X* **7**, 011030 (2017).
- [19] X. Mi, J. Cady, D. Zajac, P. Deelman, and J. Petta, *Science*, aal2469 (2016).
- [20] J. Colless, A. Mahoney, J. Hornibrook, A. Doherty, H. Lu, A. Gossard, and D. Reilly, *Physical review letters* **110**, 046805 (2013).
- [21] M. Gonzalez-Zalba, S. Barraud, A. Ferguson, and A. Betz, *Nature communications* **6**, 6084 (2015).
- [22] M. House, T. Kobayashi, B. Weber, S. Hile, T. Watson, J. Van Der Heijden, S. Rogge, and M. Simmons, *Nature communications* **6**, 8848 (2015).
- [23] N. Ares, F. J. Schupp, A. Mavalankar, G. Rogers, J. Griffiths, G. A. C. Jones, I. Farrer, D. A. Ritchie, C. G. Smith, A. Cottet, G. A. D. Briggs, and E. A. Laird, *Phys. Rev. Applied* **5**, 034011 (2016).
- [24] A. Crippa, R. Maurand, D. Kotekar-Patil, A. Corna, H. Bohuslavskyi, A. O. Orlov, P. Fay, R. Laviéville, S. Barraud, M. Vinet, M. Sanquer, S. D. Franceschi, and X. Jehl, *Nano letters* **17**, 1001 (2017).
- [25] R. C. Ashoori, H. L. Stormer, J. S. Weiner, L. N. Pfeiffer, S. J. Pearton, K. W. Baldwin, and K. W. West, *Phys. Rev. Lett.* **68**, 3088 (1992).
- [26] C. Ciccarelli and A. Ferguson, *New Journal of Physics* **13**, 093015 (2011).
- [27] F. Persson, C. Wilson, M. Sandberg, G. Johansson, and P. Delsing, *Nano letters* **10**, 953 (2010).
- [28] R. Mizuta, R. M. Otxoa, A. C. Betz, and M. F. Gonzalez-Zalba, *Phys. Rev. B* **95**, 045414 (2017).
- [29] A. Betz, S. Barraud, Q. Wilmart, B. Placais, X. Jehl, M. Sanquer, and M. Gonzalez-Zalba, *Applied Physics Letters* **104**, 043106 (2014).

- [30] B. Voisin, V.-H. Nguyen, J. Renard, X. Jehl, S. Barraud, F. Triozon, M. Vinet, I. Duchemin, Y.-M. Niquet, S. de Franceschi, *et al.*, *Nano letters* **14**, 2094 (2014).
- [31] H. Sellier, G. Lansbergen, J. Caro, S. Rogge, N. Collaert, I. Ferain, M. Jurczak, and S. Biesemans, *Applied physics letters* **90**, 073502 (2007).
- [32] J. Hornibrook, J. Colless, A. Mahoney, X. Croot, S. Blanvillain, H. Lu, A. Gossard, and D. Reilly, *Applied Physics Letters* **104**, 103108 (2014).
- [33] T. R. Stevenson, F. Pellerano, C. Stahle, K. Aidala, and R. Schoelkopf, *Applied physics letters* **80**, 3012 (2002).
- [34] N. J. Lambert, M. Edwards, C. Ciccarelli, and A. J. Ferguson, *Nano Letters* **14**, 1148 (2014).
- [35] S. Chorley, J. Wabnig, Z. Penfold-Fitch, K. Petersson, J. Frake, C. Smith, and M. Buitelaar, *Physical review letters* **108**, 036802 (2012).
- [36] K. Petersson, C. Smith, D. Anderson, P. Atkinson, G. Jones, and D. Ritchie, *Nano letters* **10**, 2789 (2010).
- [37] M. F. Gonzalez-Zalba, S. N. Shevchenko, S. Barraud, J. R. Johansson, A. J. Ferguson, F. Nori, and A. C. Betz, *Nano letters* **16**, 1614 (2016).
- [38] M. Urdampilleta, A. Chatterjee, C. C. Lo, T. Kobayashi, J. Mansir, S. Barraud, A. C. Betz, S. Rogge, M. F. Gonzalez-Zalba, and J. J. Morton, *Physical Review X* **5**, 031024 (2015).
- [39] A. Cottet, C. Mora, and T. Kontos, *Physical Review B* **83**, 121311 (2011).
- [40] R. Hanson, L. P. Kouwenhoven, J. R. Petta, S. Tarucha, and L. M. Vandersypen, *Reviews of Modern Physics* **79**, 1217 (2007).
- [41] L. Roschier, P. Hakonen, K. Bladh, P. Delsing, K. Lehnert, L. Spietz, and R. Schoelkopf, *Journal of applied physics* **95**, 1274 (2004).
- [42] T. Müller, T. Choi, S. Hellmüller, K. Ensslin, T. Ihn, and S. Schön, *Review of Scientific Instruments* **84**, 083902 (2013).
- [43] A. Aassime, G. Johansson, G. Wendin, R. Schoelkopf, and P. Delsing, *Physical Review Letters* **86**, 3376 (2001).
- [44] J. Stehlik, Y.-Y. Liu, C. M. Quintana, C. Eichler, T. R. Hartke, and J. R. Petta, *Phys. Rev. Applied* **4**, 014018 (2015).
- [45] R. Maurand, X. Jehl, D. Kotekar-Patil, A. Corna, H. Bohuslavskiy, R. Laviéville, L. Hutin, S. Barraud, M. Vinet, M. Sanquer, S. D. Franceschi, and X. Jehl, *Nat. Commun.* **7**, 13575 (2016).
- [46] A. Betz, R. Wacquez, M. Vinet, X. Jehl, A. Saraiva, M. Sanquer, A. Ferguson, and M. Gonzalez-Zalba, *Nano letters* **15**, 4622 (2015).
- [47] A. Betz, M. Tagliaferri, M. Vinet, M. Broström, M. Sanquer, A. Ferguson, and M. Gonzalez-Zalba, *Applied Physics Letters* **108**, 203108 (2016).